Atomic-Scale Corrugations in Crystalline Polypeptoid Nanosheets Revealed by Three-Dimensional Cryogenic Electron Microscopy

Xi Jiang[1]*, Morgan Seidler[1,2], Glenn L. Butterfoss[3], Xubo Luo[4], Tianyi Yu[4]. Sunting Xuan[4], David Prendergast[4], Ronald N. Zuckermann[4], Nitash P. Balsara[1,2]

1. Materials Sciences Division, Lawrence Berkeley National Laboratory, Berkeley, CA 94720, USA

2. Department of Chemical and Biomolecular Engineering, University of California, Berkeley, CA 94720, USA

3. Center for Genomics and Systems Biology, PO Box 129188, New York University, Abu Dhabi, United Arab Emirates

4. Molecular Foundry, Lawrence Berkeley National Laboratory, Berkeley, CA 94720, USA

* Corresponding author: xijiang@lbl.gov

Abstract:

Amphiphilic molecules that can crystallize often form molecularly thin nanosheets in aqueous solutions. The possibility of atomic-scale corrugations in these structures has not yet been recognized. We have studied the self-assembly of amphiphilic polypeptoids, a family of bio-inspired polymers that can self-assemble into various crystalline nanostructures. Atomic-scale structure of the crystals in these systems has been inferred using both X-ray diffraction and electron microscopy. Here we use cryogenic electron microscopy to determine the in-plane and out-of-plane structures of a crystalline nanosheet. Data were collected as a function of tilt angle and analyzed using a hybrid single-particle crystallographic approach. The analysis reveals that adjacent rows of peptoid chains, which are separated by 4.5 Å in the plane of the nanosheet, are offset by 6 Å in the direction perpendicular to the plane of the nanosheet. These atomic-scale corrugations lead to a doubling of the unit cell dimension from 4.5 to 9 Å. Our work provides an alternative interpretation for the observed Å X-ray diffraction peak often reported in polypeptoid crystals.

Amphiphilic diblock copolymers comprising amorphous and crystalline blocks form a variety of "core-shell" morphologies in solvents that dissolve the amorphous block[1-10]. The crystalline cores are often planar due to the fact that this geometry is commensurate with the underlying unit cells[1, 2, 11-14]. The question we seek to answer is how the peptoids interact with one another in the lattice and to understand their molecular conformation on the atomic scale. Polypeptoids are a family of bio-inspired polymers which comprise a similar N-substituted glycine backbone. Diblock copolypeptoids (in a wide range of molecular weight) with a hydrophilic amorphous block and a crystalline hydrophobic block from nanosheets when dissolved in water[15-22]. These crystalline nanosheets are ideally suited for atomic-scale cryogenic electron microscopy[23-25]. The molecular shape and rough packing geometry of the crystal structure has been revealed by these experiments but the atomic details are absent. The polypeptoid backbone adopts an all-*cis* configuration[20, 22, 25, 26]. The absence of folded-chain crystals in lower MW nanosheets (<6 kDa) is due to the fact that the chain lengths are sufficiently short. The hydrophobic side chains emanate from an extended backbone on both sides to form a V-shaped crystalline motif. Adjacent rows of polypeptoid molecules adopt either anti-parallel V-shaped or parallel V-shaped side chain conformations [25], depending on the chemical structure of the hydrophobic side chains and processing conditions[27, 28]. This structural information obtained thus far is based on through-plane electron micrographs coupled with atomistic molecular dynamics simulations. Complementary information (not on the atomic scale) can be obtained from from X-ray diffraction [19-22, 29, 30], neutron scattering [19, 20], and atomic force microscopy (AFM) [21, 29, 30]. These polypeptoids often form planar crystals with thicknesses in the range of nanometers thick and lateral dimensions in the range of micrometers. In addition,

crystalline polypeptoid nanosheets contain numerous defects, including poorly ordered domains and grain boundaries[31]. The through-plane cryogenic transmission electron microscopy (cryo-TEM) experiments thus far have only resolved atomic structure in two-dimensions (2D) within the nanosheet plane[25, 27, 28, 31, 32].

Electron crystallography, which is a well-established 3D reconstruction method for radiation sensitive materials, e.g. proteins, polymers, and coordination frameworks, comprises either aligning the Bragg reflections in low-dose cryo-TEM electron diffraction patterns or images obtained from ultra-thin planar crystals oriented at different tilt angles relative to the incident electron beam[33-38]. These approaches have been used to resolve the 3D structures of several systems including membrane proteins[34, 37, 39-44] and polymer single crystals[33, 35, 45-47] using XDS[48], MRC[49], or 2dx software packages[50]. Nevertheless, the averaged structural information can lead to ambiguity if the planar crystals are heterogeneous – projections of tilted samples may contain superpositions of fundamentally different crystalline motifs, especially at large tilt angles. More recently, a hybrid processing method that combines electron crystallography and single particle analysis (SPA) has been developed[51, 52]. In this approach, electron crystallography is used to obtain a approximation of the 3D structure of planar crystals. Sophisticated refinement algorithms in SPA software packages, such as Frealign[53] or Relion [54], are then used to refine and realign the local tilt geometry of unit cells to improve the spatial resolution of 3D structures. Constraints on the flatness of the crystals that reside on a supporting grid become thus far more stringent when images are collected from tilted samples compared to through-plane imaging. In through-plane images, data from flat portions of the sample can readily be sorted and averaged, reducing the effect of data from crinkled sections. In tilted samples, however, the spatial resolution of lattice structure and the local tilt geometries obtained from flat samples can easily

be affected by crinkles[55]. In order to overcome the crinkling, we applied the ultra-flat supporting grid[32], which reduces crinkles significantly, to collect data from tilted specimens. -

While the XRD measurements have been frequently used to investigate the internal ordered structure of nanosheets by comparing the fingerprint peaks with atomic models generated by DFT or MD simulations, the assignments of some structural features are still under debate [20-22, 29]. To directly reveal the structural information, which is buried in the direction parallel with the incident electron beam, in the nanosheet, images must be collected from tilted nanosheets and merged to reconstruct the 3D density map of the crystal lattice.

In this work, crystallization-driven self-assembled nanosheets were obtained by dissolving diblock polypeptoids in a mixture of solvents (THF and water) and then removing the more volatile solvent (THF) by slow evaporation. The hydrophilic blocks are exposed to water and the hydrophobic blocks, which have Br atoms in the *para* position of the phenyl group, form the crystalline core of planar sheets. We determine the structure of the polypeptoid nanosheets using hybrid electron crystallography. High-resolution cryo-TEM images are obtained from vitrified nanosheets at different tilting angles. The electron density maps of tilted nanosheets indicate the presence of structures that were not observable in the non-titled nanosheets. The analysis reveals that adjacent rows of peptoid chains, which are separated by 4.5 Å in the plane of the nanosheet, are offset by 6 Å in the direction perpendicular to the plane of the nanosheet.

The chemical structure of the amphiphilic peptoid used in this study, Nte_4-*b*-$N4Brpe_6$, is shown in Figure 1A. It comprises a hydrophilic *N*-2-(2-(2-methoxyethoxy)ethoxy)ethylglycine block (Nte) and a hydrophobic *N*-2-phenylethylglycine (N4Brpe) block bearing bromine atoms as *para*

substituents on the aromatic rings.   The N4Brpe$_6$ block forms the crystalline nanosheet, which is

stabilized in water by hydrophilic Nte$_4$ blocks. An image of the nanosheet with both
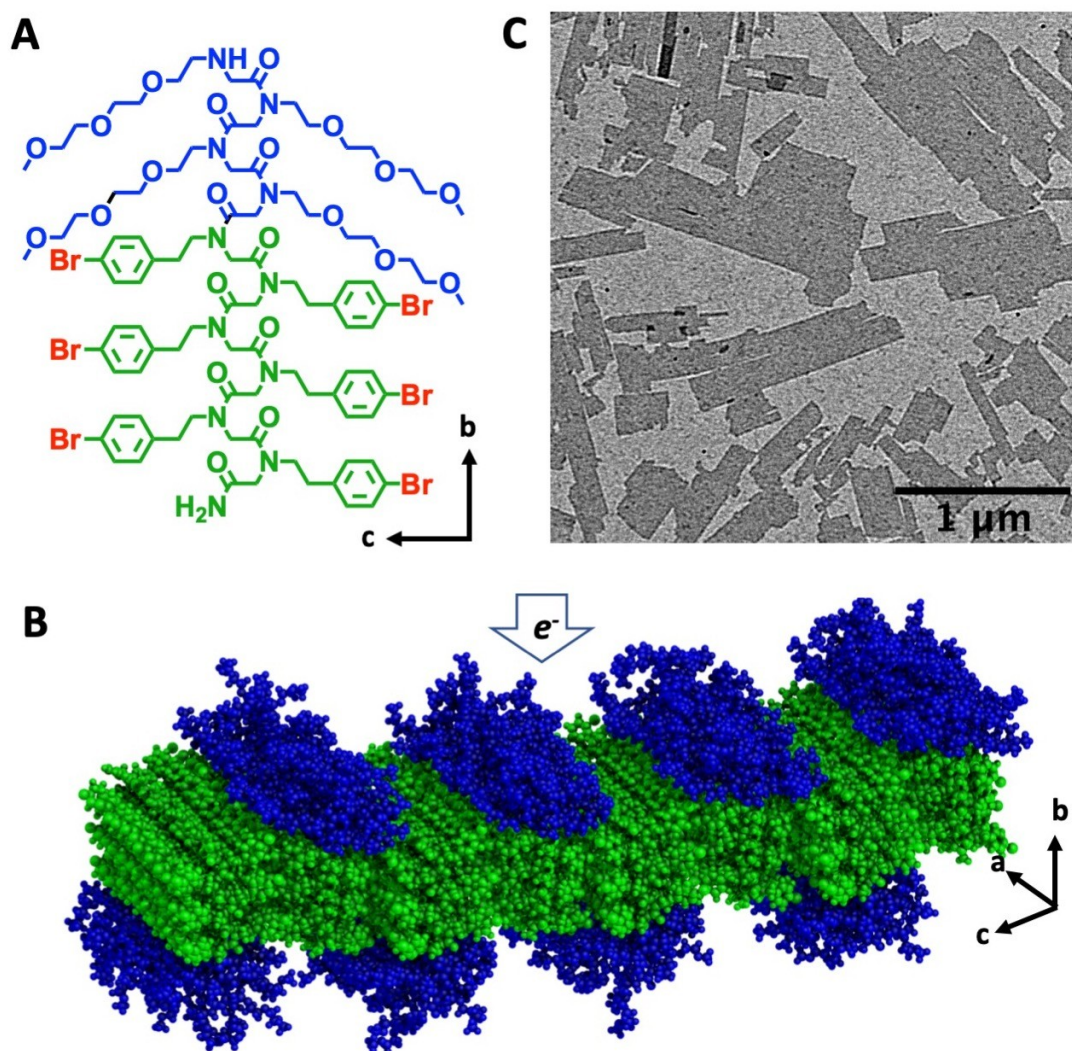

Figure 1. A The chemical structures of Nte$_4$-*b*-N4Brpe$_6$. **B.** A schematic shows the structures of

crystallization-driven self-assembled polypeptoid nanosheets. The hydrophilic blocks are shown

in blue, and the hydrophobic blocks are shown in green. **C.** A TEM micrograph obtained from

dry specimen shows the morphology of the self-assembled Nte$_4$-*b*-N4Brpe$_6$ nanosheets.

blocks, based on molecular dynamics simulation[25] validated by XRD, AFM, and 2D cryo-TEM is shown in Figure 1B. Figure 1C shows a low-resolution electron micrograph of dry Nte$_4$-b-N4Brpe$_6$, which reveals the overall shape of the nanosheets. The projection plane of the nanosheets, which reside on a carbon-supporting film, is indicated in Figure 1B.

Figure 2A shows a typical high-resolution low-dose cryo-TEM micrograph obtained from the vitrified Nte$_4$-b-N4Brpe$_6$ nanosheet (top), and the corresponding Fourier transform filtered image (bottom, one-pixel diameter filter was applied to reflections). The dark vertical lines in the bottom image represent the end view of electron dense backbones of the N4Brpe$_6$ blocks arranged in rows. The spacing between two rows is 18 Å along the c direction, see Figure 1 for definitions of a, b, and c axes. Figure 2B shows the power spectrum of the micrograph in Figure 2A. In addition to the c spacing at 18 Å, a strong row of reflections corresponding to a spacing of 4.5 Å, are seen. The spacing gives the distance between two adjacent backbones. An atomic-scale electron density map of the Nte$_4$-b-N4Brpe$_6$ nanosheet is shown in Figure 2C. The map is obtained by averaging the amplitude and phase of all reflections in the Figure 2B (see SI for details). The contrast of electron dense regions is inverted as compared to the images in Figure 2A. The bright areas represent electron dense regions in the nanosheet. The electron density map of the Nte$_4$-b-N4Brpe$_6$ nanosheet reveals that polypeptoid chains are oriented perpendicular to the plane of the nanosheet, as evidenced by the chevron-shaped end view of the glycine backbones, which adopt an all-cis conformation, in polypeptoids. The less dense arms, which emanate from the backbone, represent the side view of aromatic rings at the side chains in polypeptoids. The first two white spheres in these arms represent the side view of carbon atoms on aromatic rings. The third white sphere is the projection view of bromine atoms in a column. The whole crystal structure exhibits an anti-parallel V-shape arrangement of the molecule. It is

noteworthy that the electron density map, Figure 2C, was generated by using the electron crystallographic method to analyze one micrograph obtained from a non-tilted nanosheet. The shape of the backbone and the position of
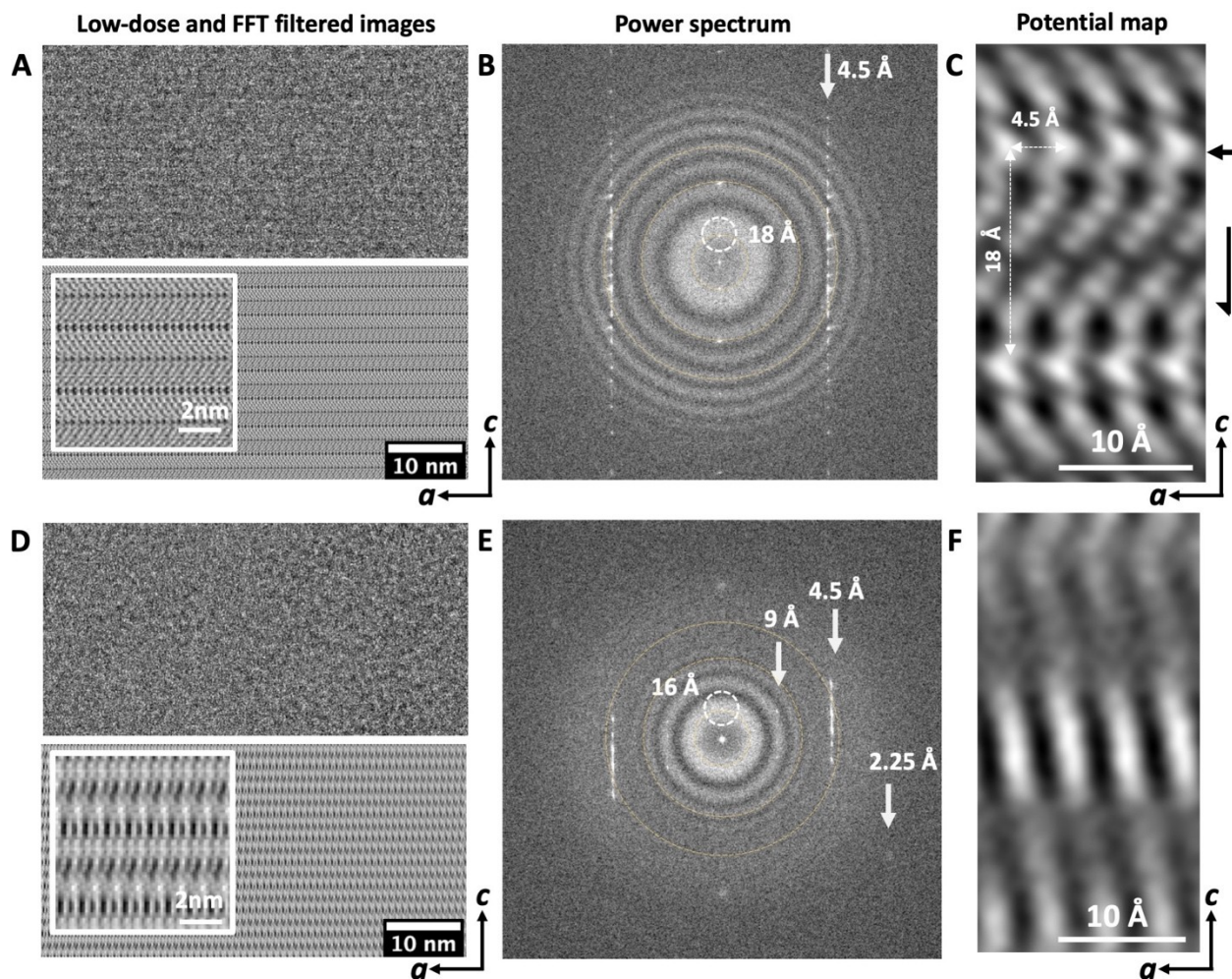

Figure 2. Structures of the self-assembled nanosheets revealed by cryo-TEM 2D images from non-tilted (**A-C**) and 30° tilted (**D-F**) specimens. **A.** A section of a low-dose cryo-EM micrograph of a vitrified hydrated Nte$_4$-b-N4Brpe$_6$ nanosheet (top) and Fourier filtered image of the micrograph (bottom) nanosheet obtained from untilted specimen. The inset image in white box shows the enlarged region of the Fourier filtered image. A mask with one-pixel diameter was applied at each reflection. **B.** The FFT of the low-dose cryo-EM micrograph in **A** showing

reflections and Thon rings due to the thin carbon support. The reflections at 4.5 Å represent the spacing between two adjacent N4Brpe$_6$ backbones in a row (*a* direction) as indicated by the arrow. The dashed circle indicates the reflection corresponding to 18 Å, which is the spacing between adjacent rows of N4Brpe$_6$ backbones (*c* direction). Resolution rings are shown in yellow dashed circles at 18 Å, 6 Å, and 4 Å, from the center. **C.** A projected electrostatic potential map was obtained by averaging the phase and amplitude information of all reflections in the micrograph. The corresponding spacings in **B** are indicated by dashed arrows. The mirror plane and the two-fold screw axis of the crystal symmetry, pmg, are shown in dark arrows. **D-F,** Analogous to figures **A-C** for a vitrified hydrated Nte$_4$-*b*-N4Brpe$_6$ nanosheet obtained from a 30° tilted specimen. Figures 2C and 2F show two unit cells along the *a* and one unit cell along the *c* directions, respectively.

atoms in side chains are more clear as compared to the image obtained by the method based on sorting and averaging about 100,000 box-shaped micrographs[25].

The lattice symmetry of crystalline Nte$_4$-*b*-N4Brpe$_6$ nanosheets exhibits a pmg planar symmetry in non-tilted cystals. Forbidden symmetries in the crystal motif lead to the absence of reflections at h=0 and k=odd, such as (0,1) and (0,3) in Figure 2B. The unit cell dimension in the plane is 4.5 x 36 Å, and it includes two molecules in a cell along the *a* and *c* directions in the non-tilted nanosheets. The mirror plane and screw axis are indicated by arrows in Figure 2C. Reflections corresponding to the forbidden symmetries are not detectable in the conventional XRD measurement [21, 22, 25, 29] but they can be directly observed by direct imaging.

In order to obtain the 3D structure of nanosheets, more images were collected from nanosheets tilted at selected angles (15°, 30°, 45°, and 60°). Each nanosheet was only imaged one time. One of the images collected at 30° is shown in Figure 2D. Images obtained at other tile angles are given in Figures S2 to S6. Interestingly, rows of reflections at 9 Å appear in the power spectrum of the tilted nanosheet as shown in Figure 2E. It is a unique feature that is not observed in the untilted crystal (Figure 2B). More importantly, it is close to a prominent peak frequently seen in the XRD measurements of crystallized polypeptoids that are similar to N4Brpe$_6$ (containing side chains with halogen-substituted aromatic rings)[21, 22, 29]. Different researchers have proposed different explanations for the presence of a peak in the vicinity of 9 Å. Zhao *et al*. carried out all-atom MD simulations of the diblock copolypeptoid, which contains the same crystalline hydrophobic block as the one in this work[20]. The sharp peak that appears at 9.1 Å in the experimental XRD was attributed by Zhao et al. to the second order of the distance (18.2 Å) between neighboring columns in the *c* direction. However, the simulated XRD, which was generated using the atomic models obtained from MD simulations, shows a much weaker peak at the same spacing. Hammons *et al*. reported the *in situ* XRD and MD simulations in the early stages of assembly of crystalline polypeptoid nanosheets, which contain different halogenated aromatic rings in hydrophobic blocks[22]. They concluded that the peak at 9 Å was not a harmonic peak from the spacing between two adjacent backbones in a row, 4.5 Å, along the *a* direction. It was attributed to the presence of herringbone packing of side chains in the *a* direction, which in fact resulted in the doubled unit cell dimension along the *a* direction.

In addition to the sharp reflections described above, more diffuse reflections are observed at the high spatial frequency in Figure 2E; such a reflection at 2.5 A is indicated in the Figure. Figure 2F shows the electrostatic potential map generated based on the image in Figure 2D.

While the alternating white and dark stripes are apparent, it is difficult to interpret the map due to the lack of dominant features related to the atomic structure of N4Brpe$_6$ (*e.g.*, aromatic rings in side chains). The images and FFTs were rotated to align the reflections for clarity. The canonical image quality (IQ) plots of the images in Figure 2C and 2F are shown in Figure S1.

To explore the molecular arrangement in the crystal, a 3D electrostatic potential map of Nte$_4$-*b*-N4Brpe$_6$ nanosheet was obtained by using a hybrid electron crystallographic processing method.[51] (See experimental section, Table S1, Figures S7 to S13 in SI for details.). This approach utilizes images obtained at all of the tilt angles. Selected slices through the 3D reconstruction are shown in the top row of Figure 3. In order to interpret these images, different views of an atomic model, which exhibits the molecular arrangement with an offset along the b direction, are shown directly below. It is noteworthy the resolution is anisotropic because of the limited tilting angles of crystals in 3D reconstruction. The resolution is higher in the *a-c* plan but lower in the *a-b* and b-*c* plans (Figure S12).
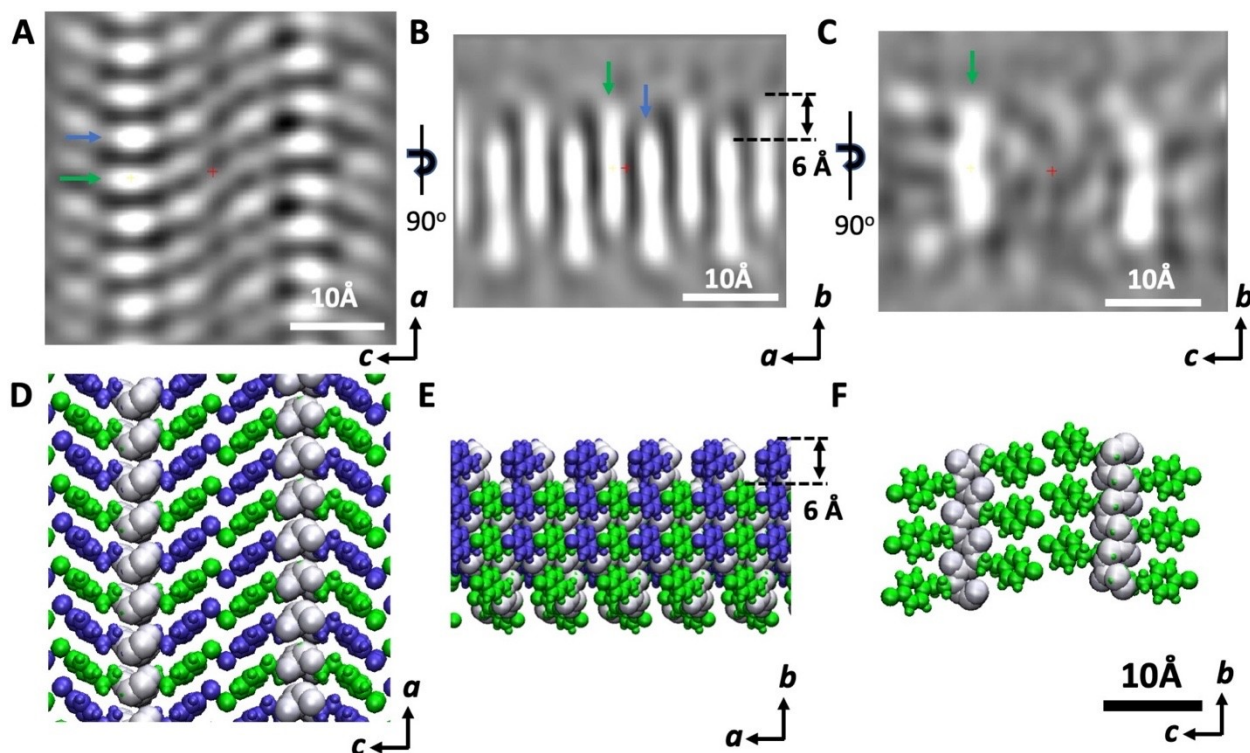
Figure 3. 3D reconstructed map of the Nte$_4$-*b*-N4Brpe$_6$ nanosheets. Electron dense regions are shown in bright, and the slice thickness is 2.8 Å. **A.** The slice view of the *a-c* plane. Green and blue arrows indicate the position of two backbones of peptoid molecules. **B.** the slice views of a *a-b* plane. The adjacent backbones indicated in **A** are shown correspondingly. A 6 Å offset is clearly observed between two backbones along the *b* direction, which is close to the length of two monomers. **C.** The slice view of the *b-c* plane. The same molecule in A and B is indicated by a green arrow. Backbones are shown in grey, and side chains are shown in green and blue in the atomic model, respectively, according the alternative spatial arrangement in a row. **D.** The view of a *a-c* plane in the atomic model. **E.** The view of a *a-b* plane shows the presence of a 6 Å offset. **F.** The view of a *b-c* plane shows two molecules in adjacent rows.

each slice in 3D reconstruction. A slice in the plane of the crystal, the *a-c* plane, is pictured in Figure 3A and the corresponding view in the atomic model is shown in Figure 3D. It shows the expected anti-parallel V-shaped motif. In this view, there is no difference between the two neighboring polypeptoid blocks along the *a* direction. For clarification, we show green and blue arrows to indicate the adjacent molecules in a unit cell along the *a* direction. Figures 3B and 3E show the cross-sectional slice in the *a-b* plane at the row indicated by the blue and green arrows, respectively. The bright "rod-like" domains represent the glycine backbones of the N4Brpe$_6$ polypeptoid blocks. It is clear that the chains at the blue arrow are displaced by about 6 Å relative to the chains at the green arrow along the *b* direction. This distance equals the length of two monomers. The *b-c* planes at the green arrow position are shown in Figures 3C and 3F. The adjacent molecules in two rows exhibit no offset along the *b* direction. The glycine backbones have the bright "sausage-like" morphology. The 9 Å XRD peak arises due to this displacement of adjacent backbones along the *b* direction, which results in the change of a unit cell from 4.5 Å x 36 Å to a supercell with the dimension at 9 Å x 36 Å (Figure S10).

The visualized surface of backbones of N4Brpe$_6$ blocks overlaid with a summed slice (4 slices thick) of the corresponding slices is shown in Figure 4A. To validate the quality of the 3D reconstruction, the atomic model was fitted into the 3D map using UCSF Chimera [56]. Figure 4B shows the atomic model fitted into the electrostatic potential map of a unit cell in the *a-c* plane. Both backbones and side chains are reasonably fitted in to the electron dense regions except the bromine substituents at the para positions of aromatic rings. Figure 4C shows the atomic model fitted into the electrostatic potential map in the *b-c* plane. Some of the aromatic rings in the side chains fit within the electron dense regions. However, the aromatic rings in the bottom of the left

row and those in the top of the right row do not fit into the electron dense regions. We posit that this inconsistency
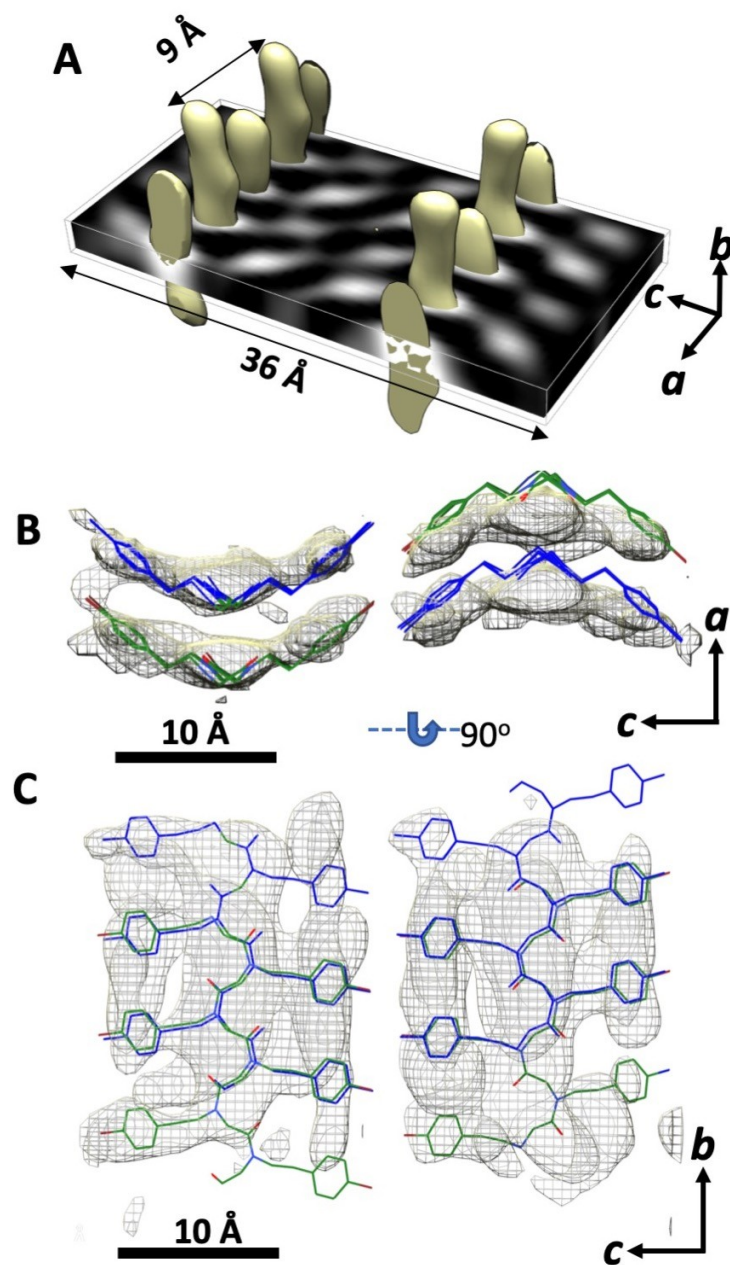

Figure 4. **A**. Visualized surface of backbones of N4Brpe6 blocks overlaid with one of the corresponding slices. **B**. The fitting map of visualized mesh surface of N4Brpe6 blocks and the atomic models in *a-c* plane. **C**. The same map rotated 90 degrees to show the *b-c* plane. The

surfaced volume of the reconstructions is shown in yellow. The atomic model of N4Brpe6 bloc

is shown in green and blue to follow the same manner. The threshold level is set to 0.02 to show

backbones in A and 0.0055 to show both backbones and side chains in B and C. The range of

threshold is from -1 x e^{30} to 1 x e^{30} in the reconstructed map with 32-bit grayscale. Stick atomic

models are shown for clarity.

arises due to the limited tilt angles used in this study, and that improving the resolution will

resolve these discrepancies. In spite of these limitations, the 3D data in Figure 4 provide

important information about the polypeptoid nanosheets that was not evident in the through

plane images.

The spatial arrangement of the polypeptoid molecules in self-assembled crystalline

nanosheets was studied using cryo-electron crystallography as a function of tilt angle. In the

non-tilted specimens (zero tilt angle), the electrostatic potential map revealed the lattice

symmetry of the unit cell, which has a two-fold screw axis along the c direction and a mirror

plane along the a direction, with the dimension at 4.5 Å x 36 Å. The correct unit cell dimension

is, however, not revealed in the images of the non-tilted specimens. In the tilted specimens, aa

additional row of 9 Å reflections was observed. 3D reconstruction of nanosheets carried out

using a hybrid electron crystallographic method indicates these reflections arise due to

displacement of the N4Brpe$_6$ polypeptoid backbones along the b direction, giving rise 9 Å x 36 Å

supercell. This study shows how structural information that is "buried" in 2D images can be

revealed by 3-D cryogenic electron microscopy. The molecular underpinnings of the corrugated

nature of the crystalline nanosheets formed by halogenated polypeptoids remain to be established.

Corresponding Authors:

* Correspondence to: xijiang@lbl.gov (X.J)

Author contributions:

Xi Jiang (X.J) and Nitash Balsara (N.P.B) designed research; X.J preformed research; Morgan Seidler (M.S) contributed to data analysis; Glenn L. Butterfoss (G.L.B), Xubo Luo (X.L), and David Prendergast (D.P) carried out molecular dynamics and DFT simulations; Tianyi Yu (T.Y), Sunting Xuan (S.X), and Ronald N. Zuckermann (R.N.Z) synthesized peptoids. X.J and N.P.B wrote the manuscript. R.N.Z and D.P modified the manuscript.

Conflict of Interest Statement:

The authors declare no competing financial interest.

Supporting Information:

Experimental section, including sample preparation, cryo-TEM data collection and processing, and X-ray diffraction simulations, and supplementary figures.

References

(1) He, W. N.; Xu, J. T. Crystallization assisted self-assembly of semicrystalline block copolymers. *Progress in Polymer Science* **2012**, *37* (10), 1350-1400. DOI: 10.1016/j.progpolymsci.2012.05.002.

(2) Yin, L. G.; Hillmyer, M. A. Disklike Micelles in Water from Polyethylene-Containing Diblock Copolymers. *Macromolecules* **2011**, *44* (8), 3021-3028. DOI: 10.1021/ma200242b.

(3) Schmelz, J.; Karg, M.; Hellweg, T.; Schmalz, H. General Pathway toward Crystalline-Core Micelles with Tunable Morphology and Corona Segregation. *Acs Nano* **2011**, *5* (12), 9523-9534. DOI: 10.1021/nn202638t.

(4) Petzetakis, N.; Dove, A. P.; O'Reilly, R. K. Cylindrical micelles from the living crystallization-driven self-assembly of poly(lactide)-containing block copolymers. *Chemical Science* **2011**, *2* (5), 955-960. DOI: 10.1039/c0sc00596g.

(5) Wang, X. S.; Guerin, G.; Wang, H.; Wang, Y. S.; Manners, I.; Winnik, M. A. Cylindrical block copolymer micelles and co-micelles of controlled length and architecture. *Science* **2007**, *317* (5838), 644-647. DOI: 10.1126/science.1141382.

(6) Zhang, L. F.; Eisenberg, A. Multiple Morphologies of Crew-Cut Aggregates of Polystyrene-B-Poly(Acrylic Acid) Block-Copolymers. *Science* **1995**, *268* (5218), 1728-1731. DOI: DOI 10.1126/science.268.5218.1728.

(7) Foster, J. C.; Varlas, S.; Couturaud, B.; Coe, Z.; O'Rei'lly, R. K. Getting into Shape: Reflections on a New Generation of Cylindrical Nanostructures' Self-Assembly Using Polymer Building Blocks. *Journal of the American Chemical Society* **2019**, *141* (7), 2742-2753. DOI: 10.1021/jacs.8b08648.

(8) Jain, S.; Bates, F. S. On the origins of morphological complexity in block copolymer surfactants. *Science* **2003**, *300* (5618), 460-464. DOI: DOI 10.1126/science.1082193.

(9) Pochan, D. J.; Chen, Z. Y.; Cui, H. G.; Hales, K.; Qi, K.; Wooley, K. L. Toroidal triblock copolymer assemblies. *Science* **2004**, *306* (5693), 94-97. DOI: DOI 10.1126/science.1102866.

(10) Zheng, J. X.; Xiong, H. M.; Chen, W. Y.; Lee, K. M.; Van Horn, R. M.; Quirk, R. P.; Lotz, B.; Thomas, E. L.; Shi, A. C.; Cheng, S. Z. D. Onsets of tethered chain overcrowding and highly

stretched brush regime via crystalline-amorphous diblock copolymers. *Macromolecules* **2006**, *39* (2), 641-650. DOI: 10.1021/ma052166w.

(11) He, X. M.; Hsiao, M. S.; Boott, C. E.; Harniman, R. L.; Nazemi, A.; Li, X. Y.; Winnik, M. A.; Manners, I. Two-dimensional assemblies from crystallizable homopolymers with charged termini. *Nature Materials* **2017**, *16* (4), 481-+. DOI: 10.1038/Nmat4837.

(12) Cha, Y. J.; Jarrett-Wilkins, C.; Rahman, M. A.; Zhu, T. Y.; Sha, Y.; Manners, I.; Tang, C. B. Crystallization-Driven Self-Assembly of Metallo-Polyelectrolyte Block Copolymers with a Polycaprolactone Core-Forming Segment. *Acs Macro Letters* **2019**, *8* (7), 835-840. DOI: 10.1021/acsmacrolett.9b00335.

(13) Chen, W. Y.; Li, C. Y.; Zheng, J. X.; Huang, P.; Zhu, L.; Ge, Q.; Quirk, R. P.; Lotz, B.; Deng, L. F.; Wu, C.; Thomas, E.L.; Cheng, S. Z. D. "Chemically shielded" poly(ethylene oxide) single crystal growth and construction of channel-wire arrays with chemical and geometric recognitions on a submicrometer scale. *Macromolecules* **2004**, *37* (14), 5292-5299. DOI: 10.1021/ma0493325.

(14) Merg, A. D.; van Genderen, E.; Bazrafshan, A.; Su, H. Q.; Zuo, X. B.; Touponse, G.; Blum, T. B.; Salaita, K.; Abrahams, J. P.; Conticello, V. P. Seeded Heteroepitaxial Growth of Crystallizable Collagen Triple Helices: Engineering Multifunctional Two-Dimensional Core-Shell Nanostructures. *Journal of the American Chemical Society* **2019**, *141* (51), 20107-20117. DOI: 10.1021/jacs.9b09335.

(15) Nam, K. T.; Shelby, S. A.; Choi, P. H.; Marciel, A. B.; Chen, R.; Tan, L.; Chu, T. K.; Mesch, R. A.; Lee, B. C.; Connolly, M. D.; Kisielowski, C.; Zuckermann, R. Z. Free-floating ultrathin two-dimensional crystals from sequence-specific peptoid polymers. *Nature Materials* **2010**, *9* (5), 454-460. DOI: 10.1038/NMAT2742.

(16) Lee, C. U.; Lu, L.; Chen, J. H.; Garno, J. C.; Zhang, D. H. Crystallization-Driven Thermoreversible Gelation of Coil-Crystalline Cyclic and Linear Diblock Copolypeptoids. *Acs Macro Letters* **2013**, *2* (5), 436-440. DOI: 10.1021/mz300667n.

(17) Sun, J.; Zuckermann, R. N. Peptoid Polymers: A Highly Designable Bioinspired Material. *ACS Nano* **2013**, *7* (6), 4715-4732. DOI: 10.1021/nn4015714.

(18) Jin, H.; Jiao, F.; Daily, M. D.; Chen, Y.; Yan, F.; Ding, Y. H.; Zhang, X.; Robertson, E. J.; Baer, M. D.; Chen, C. L. Highly stable and self-repairing membrane-mimetic 2D nanomaterials assembled from lipid-like peptoids. *Nature Communications* **2016**, *7*, 12252-12252. DOI: 10.1038/ncomms12252.

(19) Jiang, N. S.; Yu, T. Y.; Darvish, O. A.; Qian, S.; Tsengam, I. K. M.; John, V.; Zhang, D. H. Crystallization-Driven Self-Assembly of Coil-Comb-Shaped Polypeptoid Block Copolymers: Solution Morphology and Self-Assembly Pathways. *Macromolecules* **2019**, *52* (22), 8867-8877. DOI: 10.1021/acs.macromol.9b01546.
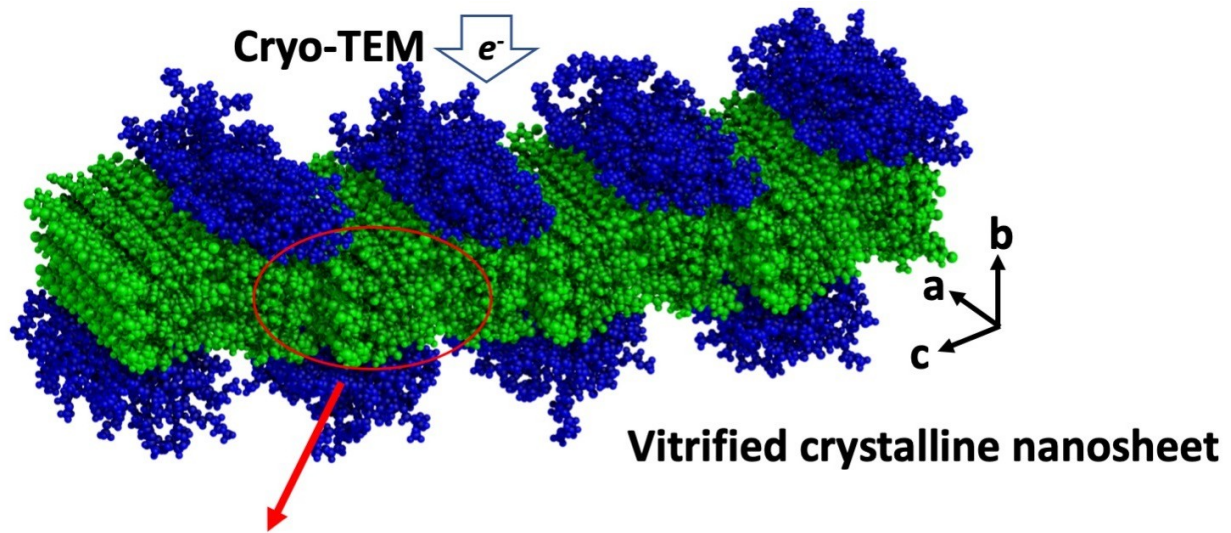
(20) Zhao, M. F.; Lachowski, K. J.; Zhang, S.; Alamdari, S.; Sampath, J.; Mu, P.; Mundy, C. J.; Pfaendtner, J.; De Yoreo, J. J.; Chen, C. L.; Pozzo, L. D.; Ferguson, A. L. Hierarchical Self-Assembly Pathways of Peptoid Helices and Sheets. *Biomacromolecules* **2021**. DOI: 10.1021/acs.biomac.1c01385.

(21) Jin, H. B.; Ding, Y. H.; Wang, M. M.; Song, Y.; Liao, Z. H.; Newcomb, C. J.; Wu, X. P.; Tang, X. Q.; Li, Z.; Lin, Y. H.; Jian, T.; Mu, P.; Chen, C. L. Designable and dynamic single-walled stiff nanotubes assembled from sequence-defined peptoids. *Nature Communications* **2018**, *9*. Article number: 270
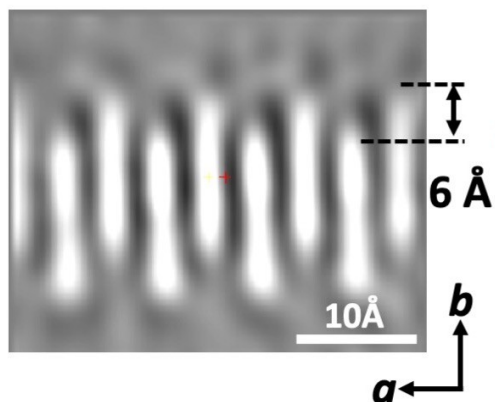
(22) Hammons, J. A.; Baer, M. D.; Jian, T. Y.; Lee, J. R. I.; Weiss, T. M.; De Yoreo, J. J.; Noy, A.; Chen, C. L.; Van Buuren, A. Early-Stage Aggregation and Crystalline Interactions of Peptoid Nanomembranes. *Journal of Physical Chemistry Letters* **2021**, *12* (26), 6126-6133. DOI: 10.1021/acs.jpclett.1c01033.

(23) Jiang, X.; Xuan, S.; Kundu, J.; Prendergast, D.; Zuckermann, R. N.; Balsara, N. P. Effect of processing and end groups on the crystal structure of polypeptoids studied by cryogenic electron microscopy at atomic length scales. *Soft Matter* **2019**, *15* (23), 4723-4736.

(24) Seidler, M.; Li, N.; Xuan, S.; Prendergast, D.; Zuckermann, R.; Balsara, N.; Jiang, X. Using cryo-TEM to study the effect of side-chain chemistry on the crystal motifs in polypeptoid nanosheets. *Microscopy and Microanalysis* **2021**, *27* (S1), 2894-2895. DOI: 10.1017/S1431927621010096.

(25) Xuan, S. T.; Jiang, X.; Spencer, R. K.; Li, N. K.; Prendergast, D.; Balsara, N. P.; Zuckermann, R. N. Atomic-level engineering and imaging of polypeptoid crystal lattices. *Proceedings of the National Academy of Sciences of the United States of America* **2019**, *116* (45), 22491-22499. DOI: 10.1073/pnas.1909992116.

(26) Greer, D. R.; Stolberg, M. A.; Kundu, J.; Spencer, R. K.; Pascal, T.; Prendergast, D.; Balsara, N. P.; Zuckermann, R. N. Universal Relationship between Molecular Structure and Crystal Structure in Peptoid Polymers and Prevalence of the &ITcis&IT Backbone Conformation. *Journal of the American Chemical Society* **2018**, *140* (2), 827-833.

(27) Jiang, X.; Xuan, S. T.; Kundu, J.; Prendergast, D.; Zuckermann, R. N.; Balsara, N. P. Effect of processing and end groups on the crystal structure of polypeptoids studied by cryogenic electron microscopy at atomic length scales. *Soft Matter* **2019**, *15* (23), 4723-4736. DOI: 10.1039/c9sm00633h.

(28) Seidler, M.; Li, N. K.; Luo, X. B.; Xuan, S. T.; Zuckermann, R. N.; Balsara, N. P.; Prendergast, D.; Jiang, X. Importance of the Positively Charged sigma-Hole in Crystal Engineering of Halogenated Polypeptoids. *Journal of Physical Chemistry B* **2022**, *126* (22), 4152-4159. DOI: 10.1021/acs.jpcb.2c01843.

(29) Jin, H. B.; Jiao, F.; Daily, M. D.; Chen, Y. L.; Yan, F.; Ding, Y. H.; Zhang, X.; Robertson, E. J.; Baer, M. D.; Chen, C. L. Highly stable and self-repairing membrane-mimetic 2D nanomaterials assembled from lipid-like peptoids. *Nature Communications* **2016**, *7*. DOI: ARTN 12252 10.1038/ncomms12252.

(30) Sun, J.; Wang, Z. W.; Zhu, C. H.; Wang, M. Y.; Shi, Z. K.; Wei, Y. H.; Fu, X. H.; Chen, X. S.; Zuckermann, R. N. Hierarchical supramolecular assembly of a single peptoid polymer into a planar nanobrush with two distinct molecular packing motifs. *Proceedings of the National Academy of Sciences of the United States of America* **2020**, *117* (50), 31639-31647. DOI: 10.1073/pnas.2011816117.

(31) Jiang, X.; Greer, D. R.; Kundu, J.; Ophus, C.; Minor, A. M.; Prendergast, D.; Zuckermann, R. N.; Balsara, N. P.; Downing, K. H. Imaging Unstained Synthetic Polymer Crystals and Defects on Atomic Length Scales Using Cryogenic Electron Microscopy. *Macromolecules* **2018**, *51* (19), 7794-7799. DOI: 10.1021/acs.macromol.8b01508.

(32) Jiang, X.; Xuan, S. T.; Zuckermann, R. N.; Glaeser, R. M.; Downing, K. H.; Balsara, N. P. Minimizing Crinkling of Soft Specimens Using Holey Gold Films on Molybdenum Grids for Cryogenic Electron Microscopy. *Microscopy and Microanalysis* **2021**, *27* (4), 767-775. DOI: 10.1017/S1431927621000520.

(33) Moss, B.; Dorset, D. L.; Wittmann, J. C.; Lotz, B. Electron Crystallography of Epitaxially Grown Paraffin. *Journal of Polymer Science Part B-Polymer Physics* **1984**, *22* (11), 1919-1929. DOI: DOI 10.1002/pol.1984.180221106.

(34) Glaeser, R. M. Electron Crystallography of Biological Macromolecules. *Annual Review of Physical Chemistry* **1985**, *36*, 243-275. DOI: DOI 10.1146/annurev.physchem.36.1.243.

(35) Dorset, D. L.; Zemlin, F. Direct Phase Determination in Electron Crystallography - the Crystal-Structure of an Normal-Paraffin. *Ultramicroscopy* **1990**, *33* (4), 227-236. DOI: Doi 10.1016/0304-3991(90)90040-S.

(36) Dorset, D. L. Electron Crystallography of Organic and Biological Molecules - Techniques and Comparison to X-Ray Crystallographic Results. *Micron* **1994**, *25* (5), 423-430. DOI: Doi 10.1016/0968-4328(94)00022-0.

(37) Renault, L.; Chou, H. T.; Chiu, P. L.; Hill, R. M.; Zeng, X. Y.; Gipson, B.; Zhang, Z. Y.; Cheng, A. C.; Unger, V.; Stahlberg, H. Milestones in electron crystallography. *Journal of Computer-Aided Molecular Design* **2006**, *20* (7-8), 519-527. DOI: 10.1007/s10822-006-9075-x.

(38) Dorset, D. L. Electron crystallography of organic materials. *Ultramicroscopy* **2007**, *107* (6-7), 453-461. DOI: 10.1016/j.ultramic.2006.03.015.

(39) Glaeser, R. M. *Electron crystallography of biological macromolecules*; Oxford University Press, 2007.

(40) Johnson, M. C.; Schmidt-Krey, I. Two-Dimensional Crystallization by Dialysis for Structural Studies of Membrane Proteins by the Cryo-EM Method Electron Crystallography. *Laboratory Methods in Cell Biology: Imaging* **2012**, *113*, 325-337. DOI: 10.1016/B978-0-12-407239-8.00015-X.

(41) Henderson, R.; Unwin, P. N. Three-dimensional model of purple membrane obtained by electron microscopy. *Nature* **1975**, *257* (5521), 28-32.

(42) Amos, L. A.; Henderson, R.; Unwin, P. N. Three-dimensional structure determination by electron microscopy of two-dimensional crystals. *Prog Biophys Mol Biol* **1982**, *39* (3), 183-231.

(43) Baldwin, J. M.; Henderson, R.; Beckman, E.; Zemlin, F. Images of Purple Membrane at 2.8 a Resolution Obtained by Cryo-Electron Microscopy. *Journal of Molecular Biology* **1988**, *202* (3), 585-591. DOI: Doi 10.1016/0022-2836(88)90288-4.

(44) Gonen, T.; Cheng, Y. F.; Sliz, P.; Hiroaki, Y.; Fujiyoshi, Y.; Harrison, S. C.; Walz, T. Lipid-protein interactions in double-layered two-dimensional AQP0 crystals (vol 438, pg 633, 2005). *Nature* **2006**, *441* (7090), 248-248. DOI: 10.1038/nature04775.

(45) Dorset, D. L. Electron Crystallography of Linear-Polymers - Direct Structure-Analysis of Poly(Epsilon-Caprolactone). *Proceedings of the National Academy of Sciences of the United States of America* **1991**, *88* (13), 5499-5502. DOI: DOI 10.1073/pnas.88.13.5499.

(46) Dorset, D. L.; Zhang, W. P. Electron Crystallography at Atomic Resolution - the Structure of the Odd-Chain Paraffin Normal-Tritriacontane. *Journal of Electron Microscopy Technique* **1991**, *18* (2), 142-147. DOI: Doi 10.1002/Jemt.1060180208.

(47) Dorset, D. L. Quantitative Electron Crystallography of Linear Polymers-Direct Phase Determination. *Abstracts of Papers of the American Chemical Society* **1992**, *203*, 10-Poly.

(48) Kabsch, W. Xds. *Acta Crystallographica Section D-Biological Crystallography* **2010**, *66*, 125-132. DOI: 10.1107/S0907444909047337.

(49) Crowther, R. A.; Henderson, R.; Smith, J. M. MRC image processing programs. *J Struct Biol* **1996**, *116* (1), 9-16. DOI: DOI 10.1006/jsbi.1996.0003.

(50) Gipson, B.; Zeng, X.; Zhang, Z. Y.; Stahlberg, H. 2dx--user-friendly image processing for 2D crystals. *J Struct Biol* **2007**, *157* (1), 64-72. DOI: 10.1016/j.jsb.2006.07.020.

(51) Righetto, R. D.; Biyani, N.; Kowal, J.; Chami, M.; Stahlberg, H. Retrieving high-resolution information from disordered 2D crystals by single-particle cryo-EM. *Nature Communications* **2019**, *10*. DOI: ARTN 1722 10.1038/s41467-019-09661-5.

(52) Scherer, S.; Arheit, M.; Kowal, J.; Zeng, X.; Stahlberg, H. Single particle 3D reconstruction for 2D crystal images of membrane proteins. *J Struct Biol* **2014**, *185* (3), 267-277. DOI: 10.1016/j.jsb.2013.12.011.

(53) Grigorieff, N. FREALIGN: High-resolution refinement of single particle structures. *Journal of Structural Biology* **2007**, *157* (1), 117-125. DOI: 10.1016/j.jsb.2006.05.004.

(54) Scheres, S. H. RELION: implementation of a Bayesian approach to cryo-EM structure determination. *J Struct Biol* **2012**, *180* (3), 519-530. DOI: 10.1016/j.jsb.2012.09.006.

(55) Booy, F. P.; Pawley, J. B. Cryo-Crinkling - What Happens to Carbon-Films on Copper Grids at Low-Temperature. *Ultramicroscopy* **1993**, *48* (3), 273-280. DOI: Doi 10.1016/0304-3991(93)90101-3.

(56) Pettersen, E. F.; Goddard, T. D.; Huang, C. C.; Couch, G. S.; Greenblatt, D. M.; Meng, E. C.; Ferrin, T. E. UCSF chimera - A visualization system for exploratory research and analysis. *Journal of Computational Chemistry* **2004**, *25* (13), 1605-1612. DOI: 10.1002/jcc.20084.
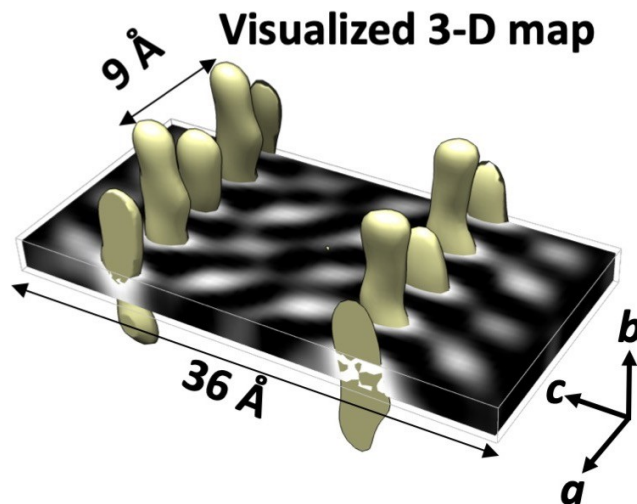
Cryo-TEM ⟶ e⁻

b
a
c

Vitrified crystalline nanosheet

3-D reconstruction

6 Å

10Å

b
a

Visualized 3-D map

9 Å

36 Å

b
c
a

Table of Contents